A computational model for nanoscale adhesion between deformable solids and its application to gecko adhesion

Roger A. Sauer [1]

Aachen Institute for Advanced Study in Computational Engineering Science (AICES), RWTH Aachen University, Templergaben 55, 52056 Aachen, Germany

Published[2] in the *Journal of Adhesion Science and Technology*, DOI: 10.1163/016942410X507588
Submitted on 20 June 2009, Accepted on 18 January 2010

Abstract

A computational contact formulation is presented that is suitable for simulating contact interaction problems at very small length scales. The contact model is based on the coarse-graining of the intermolecular forces between neighboring bodies, like van der Waals attraction, into an effective continuum contact description. The model is cast into a nonlinear 3D finite element implementation that is capable of integrating the challenges encountered in the modeling of adhesive systems.
The contact model is then applied to the dynamic modeling and simulation of the adhesion and deformation of a gecko seta based on a 3D multiscale approach. The approach spans six orders of magnitude and combines three distinct modeling levels, that describe the effective adhesion behavior at the seta scale, the spatula scale and the molecular scale. The rate-dependent pull-off behavior of adhering setae and spatulae is computed and it is shown that the model is successful in capturing pull-off forces that have been observed experimentally.

Keywords: adhesion, biomechanics, computational contact mechanics, interatomic potential, multiscale modeling, nonlinear finite element methods

1 Introduction

The research presented in this paper is motivated by modeling and studying contact and adhesion mechanisms that originate at tiny length scales but carry over to the macroscale. A prominent example is the adhesion mechanism of the gecko, that is also the central focus of this presentation. Further applications are given by MEMS (micro-electromechanical systems) adhesion [1], cell adhesion [2], rough surface adhesion [3], thin film delamination [4], and self-cleaning surfaces [5]. Small scale adhesion problems can be examined by analytical models like the Johnson, Kendall and Roberts (JKR) theory [6], or the tape peeling model of Kendall [7]. Analytical models, however, have the drawback that they are restricted to certain cases, usually the assumption of small deformations and overly simplified contact geometries. These restrictions can be overcome by finite element based computational models such as the coarse-grained contact model (CGCM) of Sauer and Li [8] which was developed for nanoscale contact and adhesion, based on the framework of non-linear continuum mechanics. This model has been validated against the JKR theory [9] as well as against molecular contact computations [10].
Several models for gecko adhesion have been proposed in the literature, amongst others by Gao

[1]Email: sauer@aices.rwth-aachen.de

et al. [11], Majidi et al. [12], Autumn et al. [13], Bhusan et al. [14], Takahashi et al. [15] and Tian et al. [16], in order to study the adhesional, frictional and self-cleaning properties of the gecko toes. Recently, also a special issue has been devoted to the subject [17]. Motivated to provide a more general and detailed model for gecko adhesion, a three-dimensional multiscale model describing the behavior of a gecko seta has been developed by the present author [18]. This paper gives a brief overview of the multiscale seta model and the underlying coarse-grained contact model. The formulation, which so far has been quasi-static, is extended to dynamics to account for inertia and damping. As a computational example, the dynamic pull-off behavior of a single gecko spatula and seta is presented. The paper also discusses some of the challenges encountered in the modeling of adhesion.

2 Challenges in the modeling of adhesion mechanisms

In the modeling of adhesion mechanisms, like the hierarchical mechanism employed by the gecko, several challenges present themselves that require an increased complexity of the modeling approach.
One challenge stems from the geometrical complexities characterizing many adhesion problems. These arise, for example, from the detailed 3D microstructure of many adhesive systems and the surface roughness of the underlying substrate. It is necessary that a certain degree of the problem geometry is captured by the model. A second challenge stems from the nonlinear kinematics associated with large deformations. In the example of the gecko seta, large bending motions can occur that cannot be described adequately by linear beam theory. Nonlinearities also stem from the adhesion law and possibly also from the material behavior. A related challenge in this regard are the jump-to-contact and jump-off-contact instabilities encountered for strong adhesion. Most nonlinearities preclude the use of analytical approaches. Another challenge is the peeling effect that occurs in many adhesion mechanisms. The gecko spatula pad, for example, gradually peels off the substrate like a thin film due to its flexibility. Neglecting the deformation and assuming that the entire pad comes off at once grossly overestimates the pull-off force. Therefore, a model like the JKR theory [6] cannot be applied to the spatula. On the other hand, a tape peeling model like the model of Kendall [7] neglects the bending stiffness of the structure and thus underestimates the pull-off force of the structure. A further challenge is the dynamical modeling of the behavior of adhesive systems. The question of rate-dependency and internal damping of adhesive systems arises. Appropriate integration algorithms are required and need to be developed. The modeling of friction of adhesive systems also poses a challenge. The interaction between adhesion and friction on rough surfaces is an open topic and appropriate laws need to be found.
The coarse-grained contact model (CGCM) is a suitable approach for addressing these challenges. So far the first three challenges have been integrated into the modeling framework of the CGCM. The extension to dynamics and its application to gecko adhesion is considered in this paper. The modeling of friction is a topic for future research.

3 Nanoscale adhesion model

This section gives a very brief overview of the finite element based CGCM developed by Sauer and Li [8, 9]. This model was developed to bridge the gap between molecular dynamics and macroscale continuum contact mechanics. According to the model, the interaction between two

deformable solids $\mathcal{B}_1$ and $\mathcal{B}_2$ is described by the interaction energy

$$\Pi_{\mathrm{c}} = \int_{\mathcal{B}_1} \int_{\mathcal{B}_2} \beta_1 \beta_2 \, \phi(r) \, \mathrm{d}v_2 \, \mathrm{d}v_1 \ , \tag{1}$$

where β_1 and β_2 denote the current molecular densities of the bodies, where $\mathrm{d}v_1$ and $\mathrm{d}v_2$ denote the deformed differential volume elements of the two bodies, and where $\phi(r)$ denotes a molecular interaction potential like the Lennard-Jones potential, defined by

$$\phi(r) := \epsilon \Big(\frac{r_0}{r} \Big)^{12} - 2\epsilon \Big(\frac{r_0}{r} \Big)^{6} \ , \tag{2}$$

which is considered in the remainder of this paper. Here ϵ and r_0 denote the separation energy and the equilibrium distance of the considered molecules. It can be shown [8] that eq. (1) leads to body forces acting within the two continua. In Sauer and Wriggers [19] it is shown that if the surface curvature radius of the bodies is more than 10 nm, the body force at $\boldsymbol{x}_k \in \mathcal{B}_k$ $(k = 1, 2)$ can be accurately expressed as

$$\boldsymbol{B}_k(\boldsymbol{x}_k) = \frac{A_H}{2\pi r_0^4 J_\ell} \left[\frac{1}{5} \Big(\frac{r_0}{r_k} \Big)^{10} - \Big(\frac{r_0}{r_k} \Big)^{4} \right] \boldsymbol{n}_{\mathrm{p}} \ , \tag{3}$$

where $r_k = |\boldsymbol{x}_k - \boldsymbol{x}_{\mathrm{p}}|$ denotes the distance between point $\boldsymbol{x}_k \in \mathcal{B}_k$ and the closest projection point, $\boldsymbol{x}_{\mathrm{p}}$, on the surface of the neighboring body, denoted $\partial \boldsymbol{B}_\ell$ $(\ell \neq k)$. Further, A_{H} denotes Hamaker's constant, $\boldsymbol{n}_{\mathrm{p}}$ denotes the outward surface normal of body $\mathcal{B}_\ell$ at $\boldsymbol{x}_{\mathrm{p}} \in \partial \mathcal{B}_\ell$ and J_ℓ denotes the determinant of the deformation gradient $\boldsymbol{F}_\ell = \operatorname{grad} \boldsymbol{\varphi}_\ell$ at $\boldsymbol{x}_{\mathrm{p}} \in \partial \mathcal{B}_\ell$. If the deformation of the neighboring body is small, we can approximate $J_\ell \approx 1$. Since the equilibrium spacing r_0 is on the order of a few Ångstroms, the body force field $\boldsymbol{B}_k(\boldsymbol{x}_k)$ will vary rapidly along the distance r_k and will only affect a thin surface layer of $\mathcal{B}_k$ that is only a few nanometers thick. For bodies larger than several nanometers, it therefore becomes useful to project the body forces onto the surface as an effective surface traction. This can be derived as

$$\boldsymbol{T}_k(\boldsymbol{x}_k) = \frac{A_{\mathrm{H}}}{2\pi r_0^3 J_\ell} \left[\frac{f_1}{45} \Big(\frac{r_0}{r_k} \Big)^{9} - \frac{f_2}{3} \Big(\frac{r_0}{r_k} \Big)^{3} \right] \boldsymbol{n}_{\mathrm{p}} \ , \tag{4}$$

where $r_k = |\boldsymbol{x}_k - \boldsymbol{x}_{\mathrm{p}}|$ now refers to the distance of the surface points $\boldsymbol{x}_k \in \partial \mathcal{B}_k$ and $\boldsymbol{x}_{\mathrm{p}} \in \partial \mathcal{B}_\ell$, and where f_1 and f_2 are functions depending on the surface curvature of body $\mathcal{B}_\ell$. If the principal curvature radii are significantly larger than the projection distance r_k, we have $f_1 \approx 1$ and $f_2 \approx 1$. A careful assessment of the accuracy of eqs. (3) and (4) is considered in Sauer and Wriggers [19].

The expressions for the finite element equations associated with formulations (3) and (4) are straightforward. Let us consider a general, three-dimensional finite element discretization of bodies $\mathcal{B}_1$ and $\mathcal{B}_2$. The procedure applied to both bodies is identical, so that we can restrict the following discussion to one body, denoted by $\mathcal{B}_k$ in general. We let n_{vel} and n_{sel} denote the total number of finite volume elements Ω_e and finite surface elements Γ_e used to discretize body $\mathcal{B}_k$ and its surface $\partial \mathcal{B}_k$, respectively. According to formulation (3), the contact force vector acting on the n_{en} nodes of element Ω_{e} is given by

$$\mathbf{f}_{\mathrm{c}}^e = \mathbf{f}_{\mathrm{b}}^e := - \int_{\Omega_{e0}} \mathbf{N}_e^T \, \boldsymbol{B}_k \, \mathrm{d}V \ , \tag{5}$$

where

$$\mathbf{N}_e = \big[\, N_1 \, \boldsymbol{I} \, , \ N_2 \, \boldsymbol{I} \, , \ \ldots \, , \ N_{n_{\mathrm{en}}} \, \boldsymbol{I} \, \big] \ , \tag{6}$$

denotes an array with the size $(3 \times 3 n_{\mathrm{en}})$ that contains the n_{en} shape functions N_i of the element. Integration (5) is carried out over the reference configuration of the element, denoted as Ω_{e0}

here. According to the alternative formulation (4), the contact force vector acting on the n_{en} nodes of surface element Γ_{e} is given by

$$\mathbf{f}_{\text{c}}^{e} = \mathbf{f}_{\text{t}}^{e} := -\int_{\Gamma_{e0}} \mathbf{N}_{e}^{T}\, \boldsymbol{T}_{k}\, \theta_{k}\, \mathrm{d}A \ , \tag{7}$$

where θ_k is a scalar that depends on the angle between the surfaces of the two neighboring bodies [8]. Integration (7) is carried out over the reference configuration of the surface element, denoted as Γ_{e0}. In order to evaluate forces $\boldsymbol{B}_k(\boldsymbol{x}_k)$ and $\boldsymbol{T}_k(\boldsymbol{x}_k)$, the closest point projection of point $\boldsymbol{x}_k$ onto the surface of the neighboring body is needed. This projection, which can cause significant difficulties, is a well studied task in computational contact mechanics [20]. The total contact-interaction force acting on body $\mathcal{B}_k$ follows from the sum of all elemental contributions, i.e.

$$\mathbf{f}_{\text{c}} = \sum_{e=1}^{n_{\text{cel}}} \mathbf{f}_{\text{c}}^{e} \ , \tag{8}$$

where either $n_{\text{cel}} = n_{\text{vel}}$ or $n_{\text{cel}} = n_{\text{sel}}$, depending on the formulation used. Due to the decay of potential (2) a cut-off radius can be considered beyond which the contributions to sum (8) are neglected. The tangent matrix associated with the contact force $\mathbf{f}_{\text{c}}$ is discussed in Sauer and Wriggers [19].
The equation of motion for a dynamic problem can be stated by the common expression

$$\mathbf{M}\ddot{\mathbf{u}} + \mathbf{f}_{\text{int}} + \mathbf{f}_{\text{c}} - \mathbf{f}_{\text{ext}} = \mathbf{0} \ , \tag{9}$$

where $\mathbf{M}$ denotes the mass matrix, $\ddot{\mathbf{u}}$ the acceleration and $\mathbf{f}_{\text{int}}$, $\mathbf{f}_{\text{ext}}$ and $\mathbf{f}_{\text{c}}$ the internal, external and contact forces of the discretized system. In general both $\mathbf{f}_{\text{int}}$ and $\mathbf{f}_{\text{c}}$ are supposed to depend on the displacement and velocity, i.e. $\mathbf{f}_{\text{int}} = \mathbf{f}_{\text{int}}(\mathbf{u}, \dot{\mathbf{u}})$ and $\mathbf{f}_{\text{c}} = \mathbf{f}_{\text{c}}(\mathbf{u}, \dot{\mathbf{u}})$, as considered in Section 4 below.

4 A multiscale model describing the adhesion of gecko setae

The above model is applied to study the adhesion of a single gecko seta. The seta is a thin, hair-like structure that branches into hundreds of fine tips, the so-called spatulae. The setae are up to 100 μm long and have a cross-sectional diameter of a few micrometers. The spatulae are around 1 μm long and have a cross-sectional diameter of around 100 nanometers. The adhesion between seta and substrate occurs predominately at the spatula pad, which forms the tip of the spatula and which is several hundred nanometers long and wide, but only a few nanometers thick. The thinness of the pad gives it great flexibility to deform and adapt to the inclination and roughness of the substrate surface.
Since the seta dimensions are several orders of magnitude larger than the range of intermolecular adhesion, a hierarchical, three-dimensional multiscale procedure is developed in Sauer [18] that spans six orders of magnitude and is able to efficiently simulate the mechanical behavior of a gecko seta during adhesion. The multiscale approach is based on the three distinct modeling levels illustrated in figure 1 and has been previously used to compute the quasi-static pull-off behavior of the gecko seta. Within the multiscale approach, the coarse-grained contact model is used to model the molecular interaction between the spatula pad and the underlying substrate. The spatula itself is modeled as a thin elastic rod with varying cross-section. At the seta level, a fractal geometry model is constructed that captures the hierarchical branching of the seta. A geometrically exact rod formulation is used to capture the nonlinear kinematics of large deformations. The constitutive behavior of the seta and spatula is described by a linear elastic isotropic material law with Young's modulus $E = 2\,\text{GPa}$ and Poisson's ratio $\nu = 0.2$. The

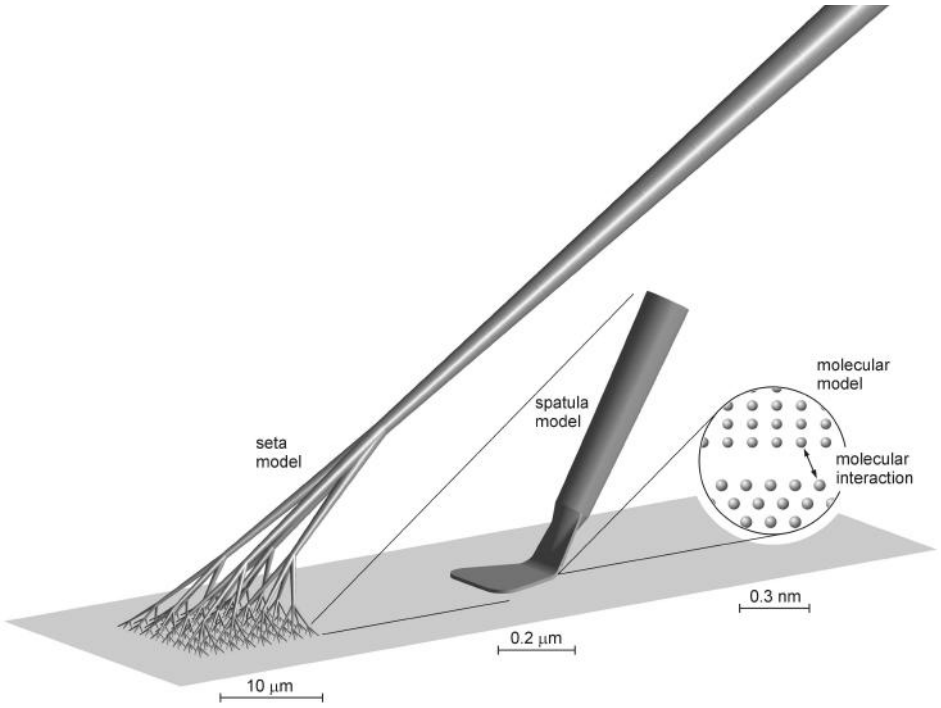

Figure 1: Mechanical multiscale model of a single gecko seta

density is assumed as $\rho = 1000\,\mathrm{kg/m^3}$. The adhesion parameters are chosen as $A_\mathrm{H} = 10^{-19}\mathrm{J}$ and $r_0 = 0.4\,\mathrm{nm}$. Further details of the model, in particular the geometry, are reported in Sauer [18].

In the following, we report how the coarse-grained contact formulation given in Section 3 is adapted to a finite rod element formulation. A detailed derivation is given in Sauer [18]. The force vector acting on rod element Ω_e, which has the initial length L_e, is found as

$$\mathbf{f}_\mathrm{c}^\mathrm{e} = -\int_0^{L_\mathrm{e}} \mathbf{N}_\mathrm{e}^T \boldsymbol{T}_\mathrm{c} \frac{w(S)\,\mathrm{d}S}{\cos\alpha} \;, \tag{10}$$

where S denotes the coordinate along the element, where w denotes the width of the element, and where $\boldsymbol{T}_\mathrm{c}$ denotes the elemental line load

$$\boldsymbol{T}_\mathrm{c} = \big[T(r_1) - T(r_2)\big]\,\boldsymbol{n}_\mathrm{s} \;, \tag{11}$$

which depends on the surface normal of the substrate, $\boldsymbol{n}_\mathrm{s}$, and on

$$T(r) := \frac{A_\mathrm{H}}{2\pi r_0^3}\left[\frac{1}{45}\Big(\frac{r_0}{r}\Big)^9 - \frac{1}{3}\Big(\frac{r_0}{r}\Big)^3\right] . \tag{12}$$

This expression is found from integrating the body force $\boldsymbol{B}_k$ (3) over

$$r_1 = r_\mathrm{M} - \frac{h}{2}\cos\alpha \;, \qquad r_2 = r_\mathrm{M} + \frac{h}{2}\cos\alpha \;, \tag{13}$$

which mark the distances of the lower and upper element boundaries from the substrate surface. Here, r_M denotes the distance between the substrate and the center axis of the element, and h denotes the element height. The angle α denotes the inclination of the element with respect to the substrate surface. We note that the force vector $\mathbf{f}_\mathrm{c}^e$ affects only the translational degrees of freedom but not the rotational degrees of freedom of the rod, since only forces but no moments

are exerted through the interaction (2). The stiffness matrix associated with $\mathbf{f}_{\mathrm{c}}^{e}$ (10) is derived in Sauer [18].
To simulate the seta behavior we also need to specify the vector of internal forces $\mathbf{f}_{\mathrm{int}}$. Here we assume that these forces can be split additively into an elastic part and a viscous part that is linear in $\dot{\mathbf{u}}$, i.e.

$$\mathbf{f}_{\mathrm{int}}(\mathbf{u}, \dot{\mathbf{u}}) = \mathbf{f}_{\mathrm{el}}(\mathbf{u}) + \mathbf{C}\dot{\mathbf{u}} \ . \tag{14}$$

The elastic forces depend on the considered finite element rod formulation. In our implementation, we have used the geometrically exact rod formulation of Simo [21] and Simo and Vu-Quoc [22], who provide an expression for $\mathbf{f}_{\mathrm{el}}$ and the associated stiffness matrix $\mathbf{K}_{\mathrm{el}}$. The damping matrix $\mathbf{C}$, used to define the viscous forces, is difficult to assess due to the lack of experimental data. For simplicity, Rayleigh damping is considered here in the form $\mathbf{C} = c_{\mathrm{m}}\mathbf{M} + c_{\mathrm{s}}\mathbf{K}_{\mathrm{el},0}$, where c_{m} and c_{s} are constants and where $\mathbf{K}_{\mathrm{el},0}$ denotes the constant stiffness matrix for $\mathbf{f}_{\mathrm{el}} = \mathbf{0}$. The mass matrix $\mathbf{M}$ is constructed as a consistent mass matrix [23].
We note that the contact-adhesion force $\boldsymbol{T}_{\mathrm{c}}$ (4) acting on the spatula pad depends only on the displacement $\mathbf{u}$ but not on the velocity $\dot{\mathbf{u}}$. On the other hand, the contact-adhesion forces acting on the tips of the seta model are rate-dependent, since they include the dynamical behavior of the spatulae. In the proposed model these forces act on the tip nodes of the discretized seta and take the form

$$\mathbf{f}_{\mathrm{c}}^{\mathrm{n}} := P(u, \dot{u})\, \boldsymbol{n}_{\mathrm{s}} \ , \tag{15}$$

where $P(u, \dot{u})$ denotes the adhesion law of the spatula, as it is obtained from the computations reported below. We note that tangential friction forces are not considered in the current adhesion model and will be included in future modeling.

5 Computational results

The multiscale seta model described above is used to analyze the dynamic pull-off behavior of the seta. Therefore, a vertical displacement $u(t)$ is applied to the shaft of the spatula and seta such that the pull-off velocity $v = \dot{u}$ is constant. The rotations and horizontal displacements are considered fixed. Figure 2 shows the deformation of the spatula during pull-off at the displacements $u = 0$, 75, 152, 191, 195 and 250 nm. The images are computed by the finite rod

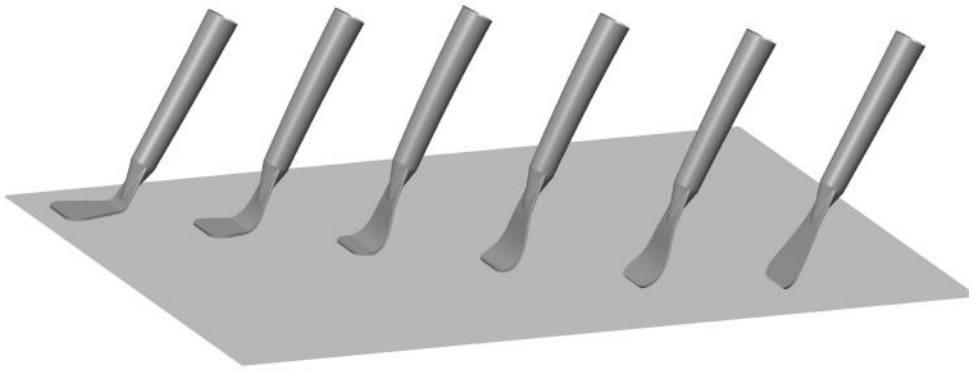

Figure 2: Pull-off of a gecko spatula with $v = 0.1$ m/s. The six configurations show the spatula deformation at the pull-off displacements $u = 0$, 75, 152, 191, 195 and 250 nm

element formulation outlined above. The pull-off force P, required to apply the displacement $u(t)$, is displayed in figure 3.a. The load-displacement curve increases up to maximum value

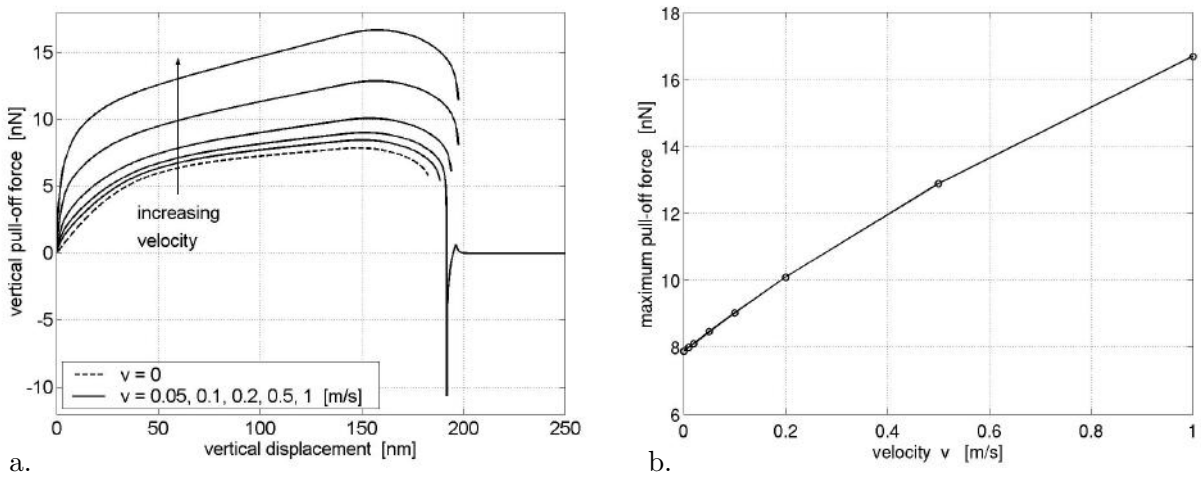

Figure 3: Spatula pull-off forces: a. Force-displacement curve $P(u, v)$, b. Velocity dependence of the maximum pull-off force

$P_{\max}$ and then drops sharply, due to the jump-off-contact characteristic common to strong adhesion. $P_{\max}$ increases with the velocity, as shown in figure 3.b. The velocities $v = 0.01$, 0.02, 0.05, 0.1, 0.2, 0.5 and 1 m/s are considered in the simulation. The dependence of $P_{\max}$ on v is not quite linear, but can be approximated very well by a quadratic function. For the considered velocities and model parameters, $P_{\max}$ lies in the range of 8 and 17 nN, which is in good agreement with the observed values by Huber et al. [24] and Sun et al. [25]. For the clarity of figure 3.a, the entire pull-off curve is only shown for the case $v = 0.1$ m/s, while the other cases are shown only prior to jump-off-contact. Their jump-off-contact behavior is similar to the case $v = 0.1$ m/s. The case $v = 0$, which has already been reported in Sauer [18], cannot be computed past jump-off-contact, due to the instability caused in quasi-static simulations. Newmark's integration method [23] has been used in the computation. To apply the velocity v at the boundary, a short time span T_{ramp} has been used to gradually increase the velocity from 0 to v. In all cases this ramp-up time is set to $T_{\text{ramp}} = 10\,\text{nm}/v$.

We note that the spatula pull-off forces depend significantly on the considered damping. Here, we have chosen stiffness proportional damping obtained from $c_{\text{m}} = 0$ and $c_{\text{s}} = 0.621/\text{ns}$. This choice corresponds to a 5% damping ratio of the first fundamental vibration mode [26], which was obtained from a linear modal analysis as $\omega = 0.161$ GHz. This choice may lead to unrealistically high damping of the higher vibration modes of the spatula. Further research, both experimental and numerical, is needed to determine the degree of damping.

In the next step, the pull-off behavior of the entire gecko seta is computed. We therefore prescribe a displacement $u(t)$ at the end of the seta trunk such that the velocity $v = \dot{u}$ is constant, similar to the spatula computation considered before. The adhesion behavior at the seta tips is now modeled by the spatula pull-off law shown in figure 3.a. The numerical data is approximated by a polynomial on a least squares basis. The same pull-off velocity range as before is considered for the seta pull-off simulation. Figure 4 shows the seta deformation for the velocity $v = 0.1$ m/s. The six configurations show the deformation at the displacements $u = 0$, 16, 22, 25, 27 and 30 μm, with an enlargement shown for $u = 27\,\mu$m. The force required for the seta pull-off is displayed in figure 5.a for the different pull-off velocities. The maximum pull-off force $P_{\max}$ increases with the velocity as is shown in figure 5.b. For large v, $P_{\max}$ can become significantly larger than the quasi-static result ($v = 0$), which was initially reported in Sauer [18]. However, the pull-off forces are still lower than 40 μN, the value reported by Autumn et al. [27]. This may be partly due to the negligence of friction in the computational model. In the simulation a ramp-up time is used to gradually increase the velocity from 0 to v. In all cases

Figure 4: Pull-off of a gecko seta with $v = 0.1\,\mathrm{m/s}$. The six configurations on the left show the deformed seta structure at the pull-off displacements $u = 0$, 16, 22, 25, 27 and $30\,\mu\mathrm{m}$. The enlargement on the right shows the deformed seta prior to jump-off, at $27\,\mu\mathrm{m}$

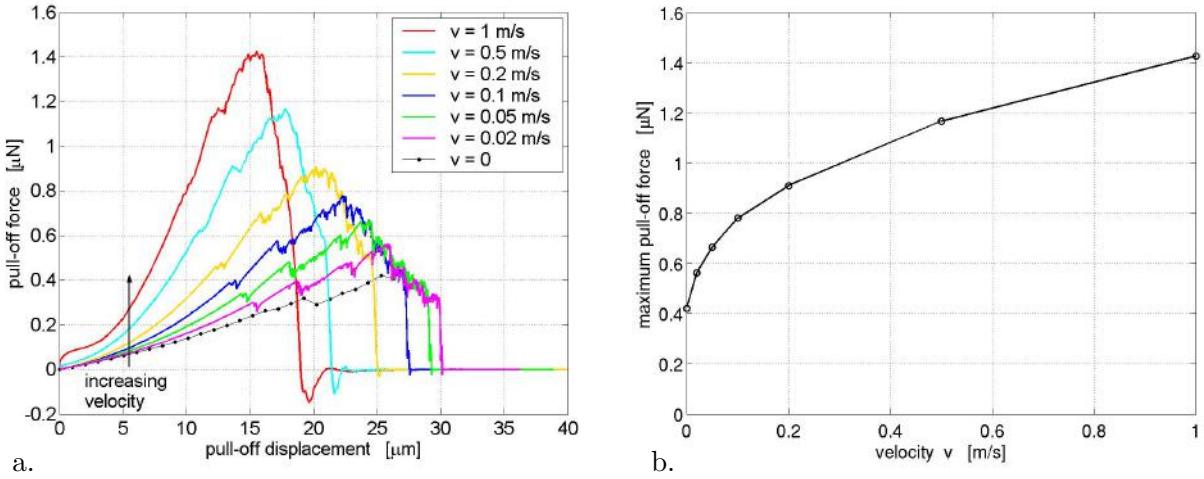

a. b.

Figure 5: Seta pull-off forces: a. Force-displacement curve $P(u, v)$, b. Velocity dependence of the maximum pull-off force

a ramp-up time of $T_{\mathrm{ramp}} = 10\,\mu\mathrm{m}/v$ was used. During ramp-up, significant inertia forces occur for $v = 1\mathrm{m/s}$ and $v = 0.5\mathrm{m/s}$, as can be seen by the initial hump in the load-displacement curve (see figure 5). Otherwise inertia has no significant effect on the simulated pull-off behavior.
As noted before, the pull-off force depends significantly on the considered damping. As in the spatula simulation, stiffness proportional damping is considered such that we have a 5% damping ratio in the first fundamental vibration mode. A linear modal analysis reveals the first natural frequency of the seta at $\omega = 0.229\,\mathrm{MHz}$. As noted above the chosen damping ratio may lead to unrealistically high damping of the higher vibration modes. On the other hand, Peattie et al. [28] have observed that the vibration behavior of setae tends to be overdamped.

6 Conclusion

This paper discusses the challenges inherent in the modeling of adhesive systems and presents an overview of the coarse-grained contact model, which offers an advantageous framework for integrating these challenges. The paper further focuses on the important model application to gecko adhesion. Rate-dependent pull-off computations of adhering setae and spatulae are shown using a hierarchical multiscale model. A major modeling difficulty lies in the estimation

of the structural damping. A further challenge lies in the computational modeling of friction. This calls for further research, in particular experiments that allow for the calibration of the parameters needed for computational modeling.

Acknowledgments

The author is grateful to Peter Wriggers and the Institute of Continuum Mechanics at the Leibniz University Hannover for supporting this research and also thanks the student Friederike Loerke for her contribution to the seta modeling.

References

[1] Zhao YP, Wang LS, Yu TX. Mechanics of adhesion in MEMS – a review. *J. Adhesion Sci. Technol.* 2003; **17**(4):519–546.

[2] Liu Y, Zhang L, Wang X, Liu WK. Coupling of navier-stokes equations with protein molecular dynamics and its application to hemodynamics. *Int. J. Numer. Methods Fluids* 2004; **46**:1237–1252.

[3] Persson BNJ, Albohr O, Tartaglino U, Volokitin AI, Tosatti E. On the nature of surface roughness with application to contact mechanics, sealing, rubber friction and adhesion. *J. Phys.: Condens. Matter* 2005; **17**(3):R1–R62.

[4] Lane M. Interface fracture. *Annu. Rev. Mater. Res.* 2003; **33**:29–54.

[5] Gao L, McCarthy TJ. The lotus effect explained: Two reasons why two length scales of topography are important. *Langmuir* 2006; **22**(7):2966–2967.

[6] Johnson KL, Kendall K, Roberts AD. Surface energy and the contact of elastic solids. *Proc. R. Soc. Lond. A* 1971; **324**:301–313.

[7] Kendall K. Thin-film peeling – the elastic term. *J. Phys. D: Appl. Phys.* 1975; **8**:1449–1452.

[8] Sauer RA, Li S. A contact mechanics model for quasi-continua. *Int. J. Numer. Meth. Eng.* 2007; **71**(8):931–962.

[9] Sauer RA, Li S. An atomic interaction-based continuum model for adhesive contact mechanics. *Finite Elem. Anal. Des.* 2007; **43**(5):384–396.

[10] Sauer RA, Li S. An atomistically enriched continuum model for nanoscale contact mechanics and its application to contact scaling. *J. Nanosci. Nanotechnol.* 2008; **8**(7):3757–3773.

[11] Gao H, Wang X, Yao H, Gorb S, Arzt E. Mechanics of hierarchical adhesion structures of geckos. *Mech. Mater.* 2005; **37**:275–285.

[12] Majidi CS, Groff RE, Fearing RS. Attachment of fiber array adhesive through side contact. *J. Appl. Phys.* 2005; **98**:103 521.

[13] Autumn K, Dittmore A, Santos D, Spenko M, Cutkosky M. Frictional adhesion: a new angle on gecko attachment. *J. Exp. Biol.* 2006; **209**:3569–3579.

[14] Bhushan B, Peressadko AG, Kim TW. Adhesion analysis of two-level hierarchical morphology in natural attachment systems for 'smart adhesion'. *J. Adhesion Sci. Technol.* 2006; **20**(13):1475–1491.

[15] Takahashi K, Berengueres JOL, Obata KJ, Saito S. Geckos' foot hair structure and their ability to hang from rough surfaces and move quickly. *Int. J. Adhesion Adhesives* 2006; **26**:639–643.

[16] Tian Y, Pesika N, Zeng H, Rosenberg K, Zhao B, McGuiggan P, Autumn K, Israelachvili J. Adhesion and friction in gecko toe attachment and detachment. *Proc. Natl. Acad. Sci. USA* 2006; **103**(51):19 320–19 325.

[17] Fearing RS, Autumn (Eds) K. Special Issue: Gecko-inspired adhesion: Theoretical and applied aspects. *J. Adhesion Sci. Techol.* 2007; **21**(12-13):1117–1341.

[18] Sauer RA. Multiscale modeling and simulation of the deformation and adhesion of a single gecko seta. *Comput. Meth. Biomech. Biomed. Eng.* 2009; **12**(6):627–640.

[19] Sauer RA, Wriggers P. Formulation and analysis of a 3D finite element implementation for adhesive contact at the nanoscale. *Comput. Methods Appl. Mech. Eng.* 2009; **198**:3871–3883.

[20] Wriggers P. *Computational Contact Mechanics*. 2nd edn., Springer, 2006.

[21] Simo JC. A finite strain beam formulation. The three-dimensional dynamic problem. Part I. *Comput. Methods Appl. Mech. Eng.* 1985; **49**:55–70.

[22] Simo JC, Vu-Quoc L. A three-dimensional finite strain rod model. Part II: Computational aspects. *Comp. Meth. Appl. Mech. Eng.* 1986; **58**:79–116.

[23] Wriggers P. *Nonlinear Finite Element Methods*. Springer, 2008.

[24] Huber G, Mantz H, Spolenak R, Mecke K, Jacobs K, Gorb SN, Arzt E. Evidence for capillarity contributions to gecko adhesion from single spatula nanomechanical measurements. *Proc. Natl. Acad. Sci. USA* 2005; **102**(45):16 293–16 296.

[25] Sun W, Neuzil P, Kustandi TS, Oh S, Samper D. The nature of the gecko lizard adhesive force. *Biophys. J.* 2005; **89**(2):L14–L17.

[26] Chopra AK. *Dynamics of Structures*. 2nd edn., Prentice Hall, 2001.

[27] Autumn K, Liang YA, Hsieh ST, Zesch W, Chan WP, Kenny TW, Fearing R, Full RJ. Adhesive force of a single gecko foot-hair. *Nature* 2000; **405**:681–684.

[28] Peattie AM, Majidi C, Corder A, Full RJ. Ancestrally high elastic modulus of gecko setal β-keratin. *J. R. Soc. Interface* 2007; **4**:1071–1076.